

## Article

# Advanced Analyses of Heating Elements Manufactured by an Optimized Arc Spraying Process

Michél Hauer <sup>1,\*</sup> , Benjamin Ripsch <sup>1</sup>, Andreas Gericke <sup>1</sup>, Werner Krömmer <sup>2</sup> and Knuth-Michael Henkel <sup>3</sup>

<sup>1</sup> Thermal Joining Engineering, Fraunhofer Institute for Large Structures in Production Engineering IGP, 18059 Rostock, Germany; benjamin.ripsch@igp.fraunhofer.de (B.R.); andreas.gericke@igp.fraunhofer.de (A.G.)

<sup>2</sup> Linde plc, Packaged Gases Germany Retail & Welding Applications/Thermal Spraying, 85716 Unterschleißheim, Germany

<sup>3</sup> Faculty of Mechanical Engineering and Marine Technologies, University of Rostock, 18059 Rostock, Germany; knuth.henkel@uni-rostock.de

\* Correspondence: michel.hauer@igp.fraunhofer.de; Tel.: +49-381-49682-225

**Abstract:** Heating elements in the automotive industry are currently produced by several thermal spray processes and materials. However, simpler spraying technologies such as arc spraying are investigated regarding technological suitability as a cost-effective alternative to plasma spraying in the production process of these components. Thus, several mixtures and combinations of alternative pressurizing gases and further modifications of an arc spray process were examined in this study. Consequently, coatings based on NiCr were produced, since this alloy is typical for heating elements. Coating properties were investigated by SEM, EDS, and resistivity measurements. The results demonstrate reduced oxygen content and improved morphology compared with the industrially used plasma-sprayed coatings. Additionally, the improved microstructure affects the surface quality and specific resistivity of the coatings positively. This allowed for laser texturing the arc-sprayed coatings successfully. It must be considered a drawback, though, that cracks partially appeared in the underlying coatings. In contrast, the temperature coefficients of resistance and the resistivities of the heating elements were superior to the conventional coatings, which can lay the foundation for a future industrial application. To further investigate this and to minimize the influence of potential sample preparation issues on the analysis results, different methods of cross-sectioning, i.e., in detail hot mounting, cold mounting, and ion beam polishing, were evaluated.

**Keywords:** arc spray; plasma spray; NiCr; alumina; heating element; automotive industry; microstructure; preparation; conductivity measurement



**Citation:** Hauer, M.; Ripsch, B.; Gericke, A.; Krömmer, W.; Henkel, K.-M. Advanced Analyses of Heating Elements Manufactured by an Optimized Arc Spraying Process. *Coatings* **2023**, *13*, 1701. <https://doi.org/10.3390/coatings13101701>

Academic Editors: Ramachandran Chidambaram Seshadri and A.K. Lakshminarayanan

Received: 21 August 2023

Revised: 19 September 2023

Accepted: 25 September 2023

Published: 27 September 2023



**Copyright:** © 2023 by the authors. Licensee MDPI, Basel, Switzerland. This article is an open access article distributed under the terms and conditions of the Creative Commons Attribution (CC BY) license (<https://creativecommons.org/licenses/by/4.0/>).

## 1. Introduction

In parallel with wear- or corrosion protection-related applications, thermally sprayed coatings or coating composites are used more and more in the electronics sector, e.g., in conductive tracks or integrated circuits [1,2], as they will allow to adaptively adjust the properties of the final product [1,3–6]. Another application area that is currently being studied in great detail is the manufacturing of electrical components in automotive engineering. Particularly complete heating systems for vehicle passenger interiors are nowadays fabricated by a variety of coating technologies due to their high efficiency. An essential component for the proper functioning of such components is the ceramic insulating coating, which is usually based on Al<sub>2</sub>O<sub>3</sub> [5]. Currently, alumina coatings are mainly produced in the industry by atmospheric plasma spraying (APS) [5,7,8]. On top of this isolating coating, a thin resistive heating coating is applied by atmospheric plasma spraying (APS). These resistive heating coatings are typically fabricated of NiCr 80/20 due to high consistency as well as low noise resulting in stable long-term electrical properties [9]. Additive-subtractive methods are increasingly used in the development

for e.g., temperature sensing or embedded microheaters [5,10]. To achieve homogeneous heating, the thermal spray NiCr coating (additive part) is usually refined by processes like laser texturing (subtractive). Atmospheric plasma spraying as a partly hot powder process, however, has some disadvantages in the production of thin resistive coatings. On one hand, there are the side process times until the plasma is stable and the deposition can be started. On the other hand, NiCr particles often oxidize strongly on an industrial scale and thus apart from a possible weak bond or cracking, partially interfere with subsequent processes, see Figure 1.

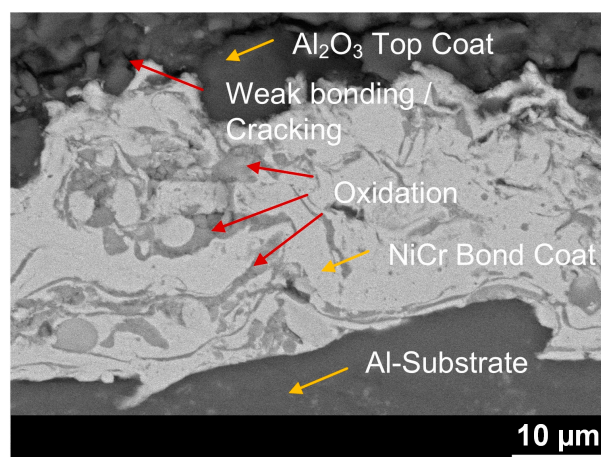


**Figure 1.** Basic coating system: Al-based substrate, NiCr bond coat, and Al<sub>2</sub>O<sub>3</sub> top coat (both sprayed by APS). For comparison, both reference NiCr resistive heating coatings using APS and arc-sprayed variations are applied onto the ceramic top coating.

Thus, simpler spraying technologies such as arc spraying (AS) are presently also being investigated for their technological suitability as a cost-effective alternative to plasma spraying in the manufacturing process for these components. Other technologies, such as HVOF spraying or wire flame spraying are potential options for achieving the desired properties too [11–14]. However, this is contrasted by higher costs due to either more expensive equipment in terms of HVOF or limited deposition in highly automatized production lines when wire flame spray is compared with arc spray. Arc spray is an established technology and a good compromise in terms of high deposition rates, low investment costs and robust technology [15,16]. For this reason, this technology was chosen in agreement with the industry partner/heater manufacturer. Yet, in case of the proposed application, it must be clarified whether such thin coatings can be structured like the plasma-sprayed coatings and to what extent this affects the underlying ceramic coating. Moreover, the typical lamellar structure with partially big splats might be problematic. Yet, own comparative tests regarding the adhesive tensile strength showed promising adhesion of NiCr 80/20 coatings deposited by arc spray compared with the typical industrial system sprayed by APS, see Table 1. Nevertheless, the different substrate materials can play a role in this regard. It should also be noted that further coatings are applied at the component level and that these values are therefore only of limited significance as a part of the entire system. The focus of the investigations will therefore lie more on the cohesive, above all electrical, properties of the coatings and heating units, i.e., after texturing.

**Table 1.** Adhesive tensile strength in MPa for NiCr 80/20 coatings dependent on spray technology and substrate type. Determined according to ISO 14916 (three specimens each).

	Atmospheric Plasma Spray (APS; on Al-Based Substrate)	Arc Spray (AS; on Mild Steel Substrate)
Tensile adhesive strength in MPa	22.4 ± 2.5	47.8 ± 0.6

Our earlier work and the related literature have shown that coatings sprayed with a mixture of nitrogen and hydrogen provide better coating properties in terms of oxidation, electrical conductivity as well as a finer overall microstructure [16,17]. Hence, solely alternative pressurizing gases and mixtures are utilized in this study. The approach in this paper can thus improve both the efficiency of the process and potentially the coating properties. The focus of the first part of the paper will therefore be on different variations of these and the effects on microstructure and functional properties. In the case of applications such as heating conductors, the coating thicknesses and masses are crucial in determining the functionality of a coating composite. For this reason, it is imperative to comply with a range of these coating properties defined in advance. As with all other coating properties presented below, the mass and thickness of the arc-sprayed coatings were therefore set in relation to the properties of the currently used plasma-sprayed coatings as a reference. Furthermore, certain critical influencing variables of the finished structured NiCr coatings must be kept in mind to allow a certain degree of flexibility in the design of the component. In addition to the resistivity of the heating element itself, this also includes the temperature coefficient of resistance (TCR) [9], which should ideally be as close as possible to the bulk material.

However, for an accurate assessment of the microstructure, the best possible preparation is necessary. Yet, the preparation of thermally sprayed coatings already differs significantly from that of bulk materials during the sectioning process. Depending on the porosity, the materials used, and the grinding and polishing steps, coating defects can be artificially enlarged or even masked or covered up [15,18–20]. The individual coating behavior further depends on the coating material and the degree of automation of grinding and polishing [15,18–20]. Consequently, a strong dependence of the assessment of the coating quality on the preparation method can be assumed. This is also evident for the mounting method. For example, cold mounting is usually recommended for thermal-sprayed coatings instead of hot mounting due to the absence of excessive pressure and heat. In the following, after all, these coatings are mechanically processed, which can possibly distort the results as described before [15,18–20]. To minimize the influence of sample preparation, alternative methods have been established in recent years, such as broad ion beam (BIB) preparation, which is analogous to focused ion beam (FIB) preparation used for the TEM [21], but covers a larger area of the sample. The advantages of this method are that almost no preliminary preparation is necessary and that temperature-sensitive materials can be processed. This means that even small and fragile structures can be prepared. Since such devices run fully automated, human influence during preparation is also minimized as far as possible [21].

In summary, the objectives of this study consist of the dual approach of, on the one hand, optimizing the coating properties of heating elements by process changes during arc spraying and, on the other hand, evaluating the influence of specimen preparation on the results of coating analyses.

## 2. Materials and Methods

The arc spray experiments were carried out by using a Sulzer Metco Smart Arc, a PPG gun and two wires of NiCr 80/20 (Metco 8450, Ø 1.6 mm; system and wires both from Oerlikon Metco Europe GmbH, Kelsterbach, Germany). In general, the substrates were prepared and coated like the reference coatings. This means, that sheets of an aluminum alloy ( $t = 3$  mm) were roughened and then coated with a NiCr 80/20 bond coat and a ceramic  $\text{Al}_2\text{O}_3$  top coat by plasma spraying with a GTV Delta torch (GTV Verschleißschutz GmbH, Luckenbach, Germany; powder process; modern three anode system). Afterwards, the arc-sprayed coatings as well as the plasma-sprayed reference coatings were then applied directly to the ceramic top coat without further substrate preparation. The experimental setups for the arc spray and plasma-sprayed reference coatings are depicted in Figure 2.

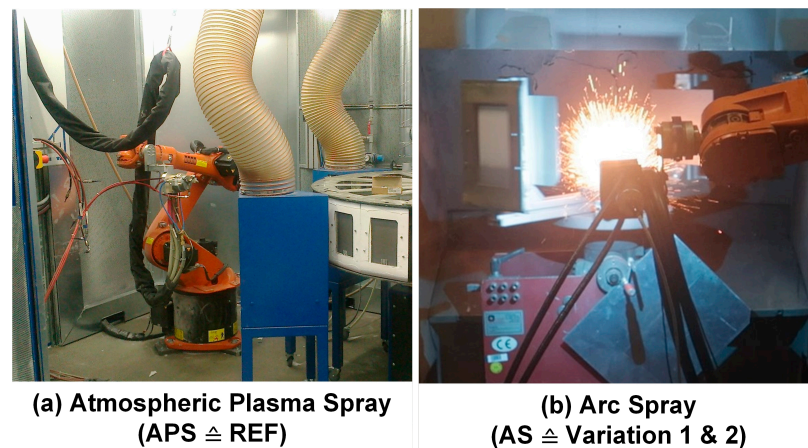


**Figure 2.** Experimental setups for (a) the atmospheric plasma-sprayed (APS REF) reference coatings and (b) arc-sprayed (AS) Variations 1 and 2. The specimens rotated, while the torches moved up and down. Kinematics were scaled accordingly to achieve equal circumferential speeds and thus deposition.

Yet, the plasma-sprayed reference coatings were fabricated on prototype components (same material) and not sheet metal. For these coatings, the same GTV Delta torch was used as described above. The spray parameters are listed in Table 2.

**Table 2.** Parameters of the arc-sprayed coating variations as well as the resulting coating mass and thickness; related to the reference coatings. The preferred parameter sets of the two variations are marked separately in the footers (S11  $\hat{=}$  S5, S12  $\hat{=}$  S12).

Specimen	Variation 1						Variation 2		
	S1	S2	S3	S4	S5 *1	S6	S7	S8 *2	S9
Wire feed rate in m/min	1.6	1.6	1.6	1.6	1.6	1.6	1.6	2.0	2.0
Arc voltage in V	28.0	28.0	30.0	30.0	30.0	30	30.0	30.0	30.0
Arc current in A	90.0	90.0	85.0	85.0	80.0	80	80.0	90.0	90.0
Stand-off distance in mm	120	120	120	100	80	60	80	80	60
Air cap	Fine Spray	High Velocity	High Velocity	High Velocity	High Velocity	High Velocity	Focused	Focused	Focused
Primary gas	N2	N2	N2 + 4% H2	N2 + 4% H2	N2 + 4% H2	N2 + 4% H2	N2 + 4% H2	N2 + 4% H2	N2 + 4% H2
Pressure in bar	4.5	4.5	4.5	4.5	4.5	4.5	4.5	4.5	4.5
Secondary gas	-	-	-	-	-	-	N2	N2	N2
Pressure in bar	-	-	-	-	-	-	3	3	3
Mass in %; related to reference	97.9	110.8	107.9	97.1	93.3	94.6	86.3	102.5	113.3
Thickness in %; related to reference	111.7 $\pm$ 18.7	131.9 $\pm$ 12.4	127.1 $\pm$ 26.7	123.9 $\pm$ 11.0	113.6 $\pm$ 7.3	111.7 $\pm$ 18.7	131.9 $\pm$ 12.4	127.1 $\pm$ 26.7	123.9 $\pm$ 11.0

\*1. Parameter set S5 corresponds to S11: Mass  $92.8 \pm 1.4\%$ ; Thickness  $109.1 \pm 23.5\%$ ; \*2. Parameter set S8 corresponds to S12: Mass  $101.8 \pm 2.4\%$ ; Thickness  $118.6 \pm 15.5\%$ .

It is visible that Variation 1 (S1–S6) was about the use of various air caps, gas types, as well as stand-off distances (SOD), while the aim of Variation 2 (S7–S9) was to further

optimize gas flow by use of a secondary gas. For Variation 1, the composition of the gas was varied because different amounts of hydrogen have additional reducing effects as well as add energy to the process for improved particle adhesion. In addition, the air caps as well as the SOD were adjusted to specifically influence the particle impact behavior and thus the cohesion of the coatings. For Variation 2, the wire feed rate of specimens S8 and S9 was increased slightly in order to achieve a proper coating mass. While specimens S1 to S9 were part of the parameter determination study (1 substrate each), series S11 and S12 (10 substrates each) are the preferred parameter sets of the two variations with respect to directly measurable coating properties, particularly mass, surface quality, and resistivity. Process kinematics were maintained the same as for the plasma-sprayed reference coatings, i.e., the sample sheets were rotated and coated with the same number of passes and by an identical robot traverse speed.

Following the spray process, the coating masses were determined using one sample each, with the exception of series S11 and S12 (10 samples each), using an SBS-LW-2000 A precision balance (Steinberg Systems, Zielona Góra, Poland). In addition, the coatings were visually checked with a CANON EOS 700D and ImageAccess software (Imagic Bildverarbeitung AG, Glattbrugg, Switzerland) with respect to the sample surface.

The specific electrical resistivity of the coatings was examined by four-terminal method using a Loresta GX MCP-T700 system (Mitsubishi Chemical Analytech Co. LTD, Kanagawa, Japan; constant current 10 mA), with 7 values recorded at 6 measurement points for each sample, see Figure 3.

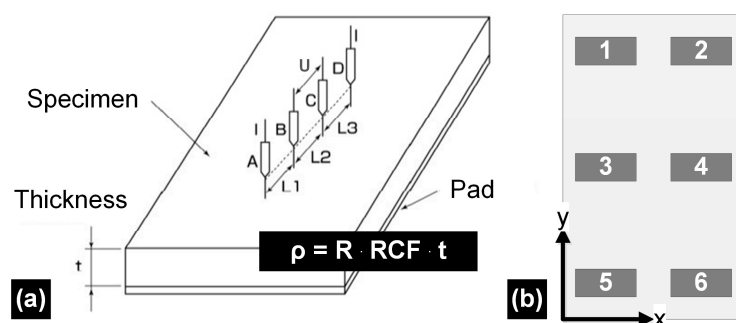


**Figure 3.** (a) Principle of the four-terminal measuring method. The specific electrical resistivity  $\rho$  is influenced by correction factor RCF (geometry, measuring position) and thickness  $t$ . (b) Measuring scheme in top view. For compensating differences in electrical energy depending on measuring position and geometry, each measuring point has its own RCF, which was determined in advance.

Since coating thickness has a major influence on the calculation of the resistivity, the corresponding values were used for samples S1 to S9. For S11 and S12 the available data are more reliable, since for these the mean values of 3 specimens were applied. Attention was paid to the coated substrates with the largest, the smallest, and the medium coating mass. In this manner, the entire spectrum of the test series is well represented. However, all coating thicknesses were only determined at the same spot by means of a microsection, as described subsequently, and not at each single measuring point following Figure 3b.

After spraying, the specimens were textured with a laser (Rofin D100, ROFIN-SINAR Laser GmbH, Hamburg, Germany), just like the plasma-sprayed coatings in industrial application, so that a geometrically defined pattern in two distinguishable loops could be obtained on the coatings. As the controlled heating would now take place by applying a voltage, the coatings can henceforth be termed heating conductors or heating elements.

The surfaces of the specimens were inspected visually (same equipment as described above). Since the temperature coefficient of resistance (TCR) and the resistivity of the heating conductor are key properties of the entire heating unit, they were measured after texturing. For this purpose, the resistivity was measured using a digital multimeter at room temperature and at 140 °C, after contacting the textured coatings via an additional copper coating onto which contact wires were soldered. Whereas the resistivity of the heating unit

can be considered as the product of measured ohm resistance and coating mass, the TCR is computed as described in [9].

For microstructural analyses of the previously described variations, the samples were first hot-mounted (HM) using an ATM Opal 410 Hot Mounting Press (ATM GmbH, Mammelzen, Germany) and then ground and polished stepwise (6  $\mu\text{m}$ , 3  $\mu\text{m}$  suspensions, finally oxide polish). The coating thickness was analyzed using a Leica DM6000M optical microscope (OM) (Leica Microsystems GmbH, Wetzlar, Germany) and the ImageAccess software tool, taking 5 readings, 3 times, for each sample. Moreover, a JEOL JSM-IT100 scanning electron microscope (SEM) (JEOL Germany GmbH, Freising, Germany; accelerating voltage 20 kV, backscatter detector) was used for coating thickness measurements of the reference samples with 3 times 7 values for each sample.

The coating morphology was investigated representatively by SEM analyses (see above for type and conditions) at various magnifications at 3 spots in each section. In addition, energy dispersive X-ray spectrometry (EDS) was performed at the same 3 locations within the cross-sections of the arc-sprayed and reference coatings using a JEOL Dry SD25 (JEOL Germany GmbH, Freising, Germany; accelerating voltage 15 kV). This allowed the local chemical composition of the coatings to be identified. Specifically, the oxygen content was examined exclusively in the NiCr coating, which was defined as region of interest (ROI) for the analysis, see Figure 4. This enabled a quantitative side-by-side comparison of the coatings.

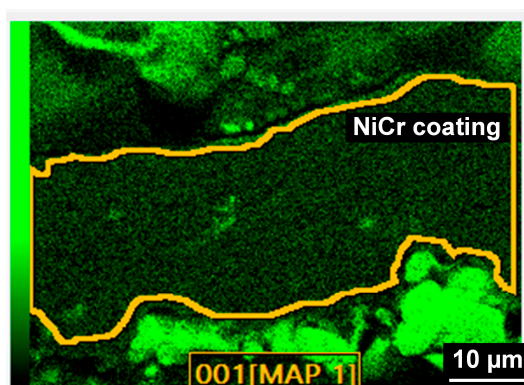


**Figure 4.** EDS mapping of oxygen inside the NiCr coating as region of interest (ROI). It can be seen, that the largest amount of the element is outside the NiCr coating.

For the sake of comparing different preparation methods in the second part of this work, some parts of the same samples (S11, S12) were (I) additionally cold-mounted (two-phase system: liquid hardener and powder resin) and gradually ground and polished (6  $\mu\text{m}$ , 3  $\mu\text{m}$  suspensions, finally oxide polish). The plasma-sprayed reference coatings were also cold-mounted like the arc-sprayed samples S11 and S12.

For further comparison purposes, segments of the same specimens S11 and S12 were (II) ion beam polished (IP) using a JEOL cross-section polisher (JEOL Germany GmbH, Freising, Germany). This was carried out by mechanically cutting sample parts first. Subsequently, the specimens were polished using a voltage of 5 kV for 8 h in a cycle of 45 s each using the electron beam and a 15 s pause. Afterwards, characterization of these specimens was carried out by OM, SEM, and EDS using the same equipment and parameters as described before, while only magnifications were different for microscopy.

Finally, SEM images (type and conditions see above) and the software ImageJ (National Institutes of Health, USA; using Despeckle filter in the ROI, normalization and finally the Trainable Weka Segmentation tool) were used for examining the content of porosity/oxidation/cracks inside the coatings for every preparation method and for both materials, the NiCr coatings (magnification 2000 $\times$ ) and the underlying ceramic  $\text{Al}_2\text{O}_3$  coating (magnification 500 $\times$ ). Three images were taken for the hot-mounted and cold-mounted specimens, while it was one image for the ion beam polished specimens. However, due to

the much larger area for the latter one, the examined specimen area was comparable in size. This procedure was also carried out for HM samples from the first part of the study, i.e., for the arc-sprayed coatings.

### 3. Results

The following section is divided into (I) the evaluation of the coatings in terms of electrical properties and relationship to microstructural conditions, and (II) the advanced microstructural evaluation using more sophisticated preparation method.

#### 3.1. Electrical and Structural Features

##### 3.1.1. Characteristics and Specific Resistivity of the Coatings

First, the coating masses were near the reference coatings with a maximum deviations of approx. 14%, see Table 2. With respect to the standard deviation of the plasma-sprayed reference coatings, which is about 8.3%, most of the arc-sprayed specimens are predominantly in the objective range for coating mass. The specimens S2 of Variation 1 as well as S7 and S9 of Variation 2 are not within this desired area. Regarding the thickness of the reference coatings and their standard deviation of 22.7%, the samples S2, S3, and S4 of Variation 1 are outside of this range, while S8 of Variation 2 has a high scatter, see Table 2.

Similar observations can be made with the surfaces in the as-sprayed state, see Figure 5.

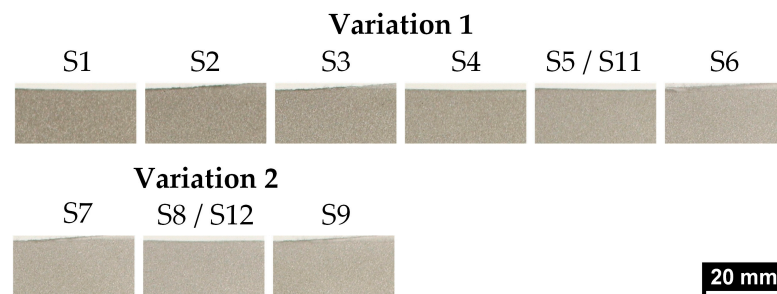


Figure 5. Surfaces of the specimens in the as-sprayed state for Variation 1 (top) and Variation 2 (bottom).

Hence, all surfaces are very bright and quite regular in appearance. The surfaces of the specimens having the smallest stand-off distance had a partly irregular coating deposition, which resulted in a certain degree of staining. Variation 2, however, shows remarkably brighter structures than Variation 1, which suggests a possibly lower degree of oxidation of these coatings.

The results of the specific resistivities vary between Variations 1 and 2, see Figure 6.

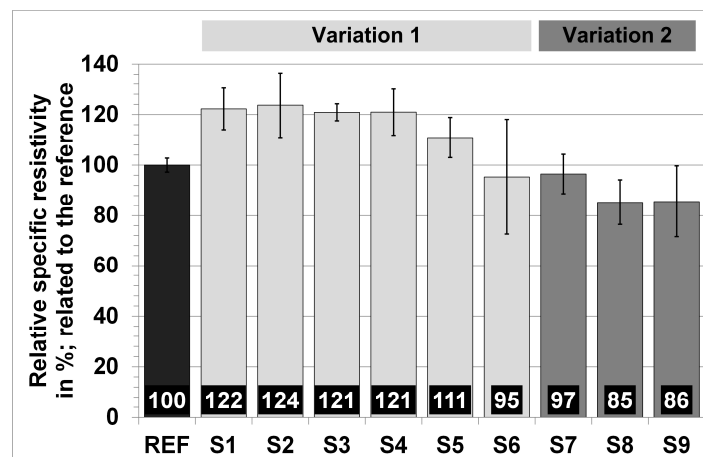
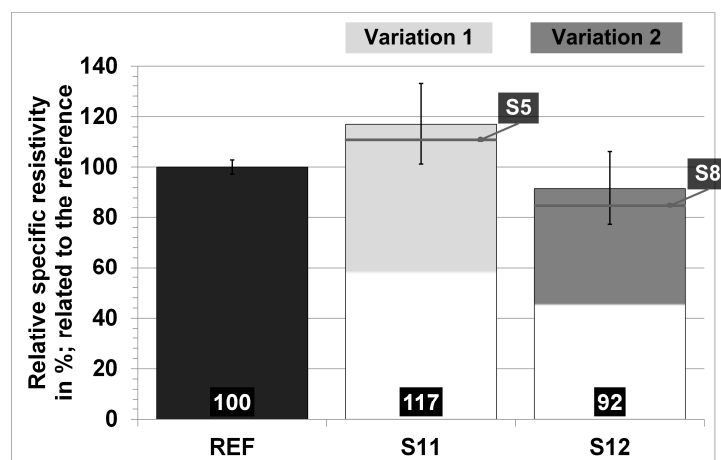


Figure 6. Relative specific resistivity and standard deviation of the arc-sprayed coatings S1 to S9; related to the value of the reference coatings (APS; REF ≅ 100%).

For Variation 1, all values, apart from S6, are higher than for the reference coatings and lie in a range of about 10% to 30% above the reference value, when the standard deviation is considered too. In addition, the standard deviation of sample S6 is approximately twice as high as for the other coatings. The parameter set S5 is found to be closest to the reference, but has a reasonable standard deviation compared with the coatings of Variation 1. In contrast, all values of Variation 2 are below the reference coating levels. While S9 has a higher standard deviation than the other samples, S7 and S8 are almost equal in spread. Nevertheless, the values differ greatly, as S7 is close to the reference, while S8 has the lowest resistivity of all coatings. Taking all this into account, the parameter sets S5 for Variation 1 and S8 for Variation 2 were considered as preferred variants for further investigations with respect to the directly determinable properties of the coatings, like mass, thickness, surface quality, and resistivity. This is confirmed by Figure 7.



**Figure 7.** Relative specific resistivity and standard deviation of the arc-sprayed coatings S11 and S12; related to the value of the reference coatings (APS; REF  $\hat{=}$  100%).

For both preferred variants S11 and S12, slightly higher resistivity values are obtained compared with the values already determined for samples S5 and S8. The standard deviations are very similar. In direct comparison, S12 exhibits a lower resistivity, which is why, analogous to the surface qualities, coatings with lower oxide contents are more likely to be expected for this series.

### 3.1.2. Representative Microstructural Features

The microstructure of the reference coatings as well as for the preferred variants of the arc-sprayed variants is presented in Figure 8.

Overall, all NiCr coatings are bonded well to the underlying ceramic coating, as can be seen in Figure 8a. A few small horizontal cracks appear to be visible within the NiCr coatings of specimens S11 and S12. In contrast, the ceramic coatings underneath the two arc-sprayed coatings are subject to cracking to a much greater extent. In addition, the ceramic coatings by themselves obviously have a more irregular surface than the reference samples. This also influences the arc-sprayed coatings on the top surface, some of which exhibit an irregular coating structure and topology, which is particularly visible in sample S11. However, looking at the coating thickness, sample S11 is obviously close to the reference, while sample S12 is thicker. This is confirmed by the values in Table 1.

At first glance, the detailed microstructural features of the reference coatings show a mostly lamellar coating structure with only a few partially molten particles, see Figure 8b. These reference coatings are also remarkable for their extensive oxide formation, which has a dark gray appearance. Not only linear oxide structures can be seen, but also larger oxidized areas with irregular shapes. Additionally, some horizontal cracks and material separations as well as irregularities can be seen.

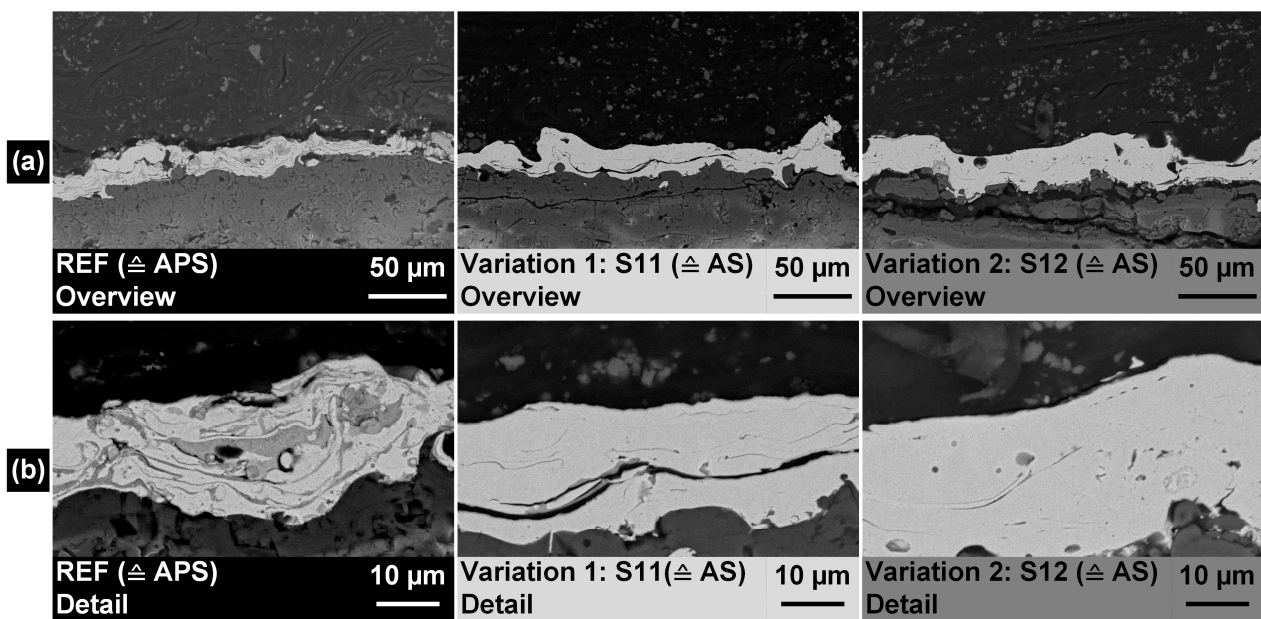


**Figure 8.** (a) Overview of the microstructure of the reference coatings (REF  $\hat{=}$  APS) and the preferred variants S11 (Variation 1  $\hat{=}$  AS) and S12 (Variation 2  $\hat{=}$  AS). (b) Detailed Microstructure of the same specimens. While the NiCr coatings are in the middle, the ceramic coating is visible below. Small horizontal cracks can be seen in the arc-sprayed coatings, while they are larger in the ceramic coating.

Specimen S11 also shows a distinct lamellar structure with solely a few partly molten particles, see Figure 8b. In contrast to the reference coatings, however, these arc-sprayed coatings demonstrate only very low detectable oxide contents. The oxides are conventionally arranged in lines and small in size. The rest of the coating is mainly characterized by the noticeable particle boundaries. Finally, a material separation at a particle interface is clearly visible, which in part coincides with the oxide formation.

Similar to the previous samples, S12 is also characterized by a lamellar structure with only a few partially molten particles. However, in an immediate comparison with the reference coatings and S11, the oxide content of the coatings is even more reduced. As a matter of fact, hardly any linearly shaped oxides can be seen, the detectable oxides seem to be rather circular and very small in dimension. The rest of the coating, apart from a few material detachments, is predominantly characterized by a uniform appearance without distinct particle boundaries.

### 3.1.3. Oxygen Content

The measurements of the oxygen content for both arc-sprayed variations as well as the reference coatings are displayed in Figure 9.

In general, the reference coatings not only show increased oxygen contents in comparison to the arc-sprayed coatings, but also higher standard deviations. Overall, the measurements of oxygen confirm the representative results already presented.

Even sample S1 with the highest oxygen content in the entire test series has an oxygen value reduced by about 66% compared with the reference coatings. In the following, the oxide content is reduced even further within Variation 1 up to a maximum of about 81%, see Figure 9. The minimum values are found in the samples S2 and S6, with only about 19% of the oxygen value of the reference coatings and small standard deviations. However, S5, as basic parameter, and the preferred variant S11 exhibit only insignificantly higher oxygen values of 20% and 21%, respectively. Nevertheless, it must be noted that this parameter variant obviously has the largest scatter occurring in Variation 1.

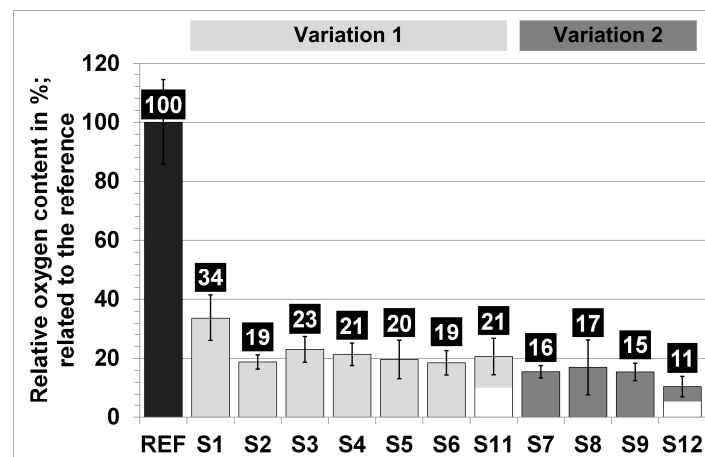


**Figure 9.** Relative oxygen content and standard deviation of the arc-sprayed coatings determined by EDS; related to the value of the reference coatings (APS; REF  $\hat{=}$  100%).

In comparison to Variation 1, Variation 2 reveals a further reduction in oxygen contents and, with the exception of S8, even lower standard deviations, see Figure 9. Regarding the samples for parameter determination S7 to S9, the result is a relatively constant average value of approx. 16% of the initial oxygen content. Interestingly, for sample S12, which has identical parameters as sample S8, an even further reduced value of 11% can be determined. At the same time, scattering of the values is lower despite the higher number of samples. Furthermore, specimen S12 is clearly superior to specimen S11 in terms of oxidation level and standard deviation. It even has the lowest value within the entire test series, which is consistent with the representative analyses of the micro-sections in the previous section.

#### 3.1.4. Texturing and Examination of the Heating Conductors

All the samples could be textured just as successfully as the reference coatings, see Figure 10. Thus, no anomalies were observed during the texturing process. The surfaces obviously changed in brightness and in surface morphology. The specimens of Variation 2 seem to be less influenced by texturing than those of Variation 1.

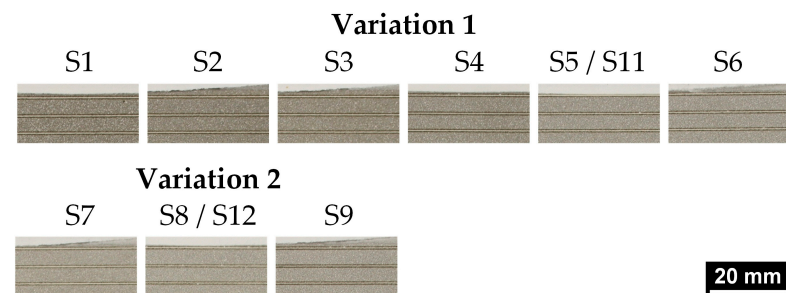


**Figure 10.** Surfaces of the specimens in the laser-textured state for Variation 1 (top) and Variation 2 (bottom).

The results of the measurements of TCR and resistivity regarding the textured heating units are displayed in Figure 11. First, when comparing the arc-sprayed coatings with the reference coatings, contradictory trends can be observed, i.e., while the values for the TCR fall strongly, increased measured resistivity levels can be observed.

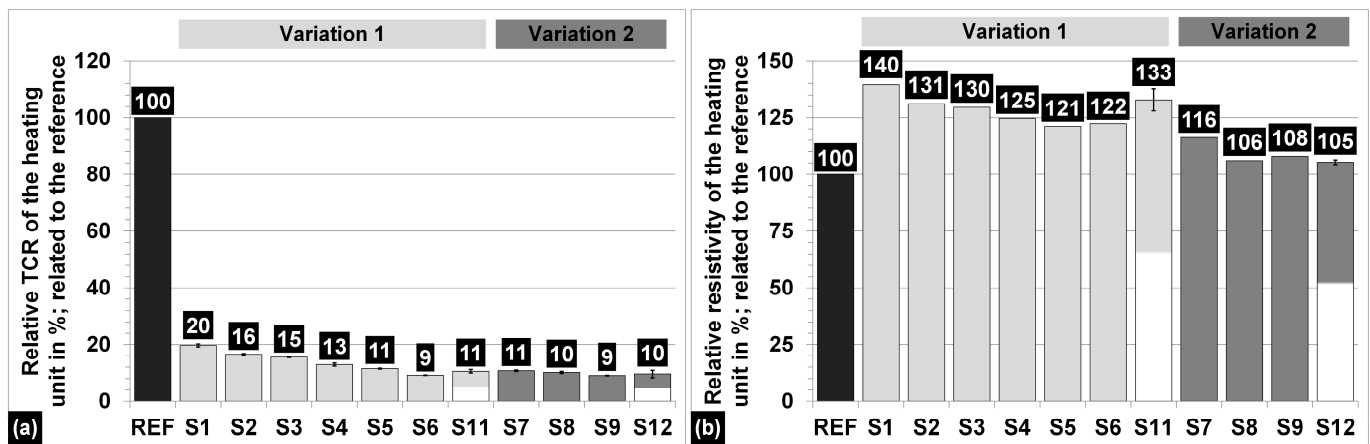


**Figure 11.** (a) Relative TCR and (b) relative resistivity of the heating unit for all the structured specimens; related to the value of the reference coatings (APS; REF  $\hat{=}$  100%).

The lowest TCR value for Variation 1 is obtained for sample S6, while the base Variation S5 and the preferred variant S11 show only slightly higher numbers. That observation is in line with the earlier results on oxygen content. The straight comparison of Variations 2 and 1 also shows a tendency towards an even smaller and constant mean value. In this case, the differences within Variation 2 are not significant. However, the two preferred variants S11 and S12 show very similar values, see Figure 11a. Additionally, the scattering of the measurements is almost negligible, which in turn correlates with the unremarkable texturing process.

The trends identified for the other measurement results can also be observed for the resistivity, see Figure 11b. While the specimens of Variation 1 tend to have higher resistivity values, those of Variation 2 are lower and more constant overall. Interestingly, the resistivity values of Variation 2 lie only slightly above the reference coatings. While the mean value for the preferred variant S11 is slightly higher than the value determined for the corresponding sample S5, the values of S8 and S12 are almost identical for Variation 2. The displayed scattering is also smaller for S12 than for S11.

### 3.2. Comparison of Preparation Methods on the Example of the Arc-Sprayed Variations and the Underlying Plasma-Sprayed Ceramic Coating

#### 3.2.1. Qualitative Microstructural Analyses

Figure 12 provides an overview of the differently prepared coatings in the laser texturing area.

First, it can be noted that, analogous to the previous investigations in section “Representative Microstructural Features”, there are partly long horizontal cracks in the  $\text{Al}_2\text{O}_3$  coating for the HM specimens. Cracks, albeit smaller, are equally pronounced near the texturing edges. In contrast, no continuous cracks can be observed in the  $\text{Al}_2\text{O}_3$  for the CM specimens, while smaller cracks continue to occur near the edges of the texturing. In contrast, no cracks at all are observed for the IP samples. A special feature is also the recognizable interface from prepared to non-prepared area as well as some artifacts in the ceramic coating. Furthermore, it is clearly visible that the IP samples have a very uniform morphology with only little and small pores in the  $\text{Al}_2\text{O}_3$  coating. For the CM and HM samples, on the other hand, large-scale extrusions from the coating are evident.

A more detailed view with higher magnification for NiCr and  $\text{Al}_2\text{O}_3$  is shown in Figure 13, which confirms the basic findings gained from the overview images.

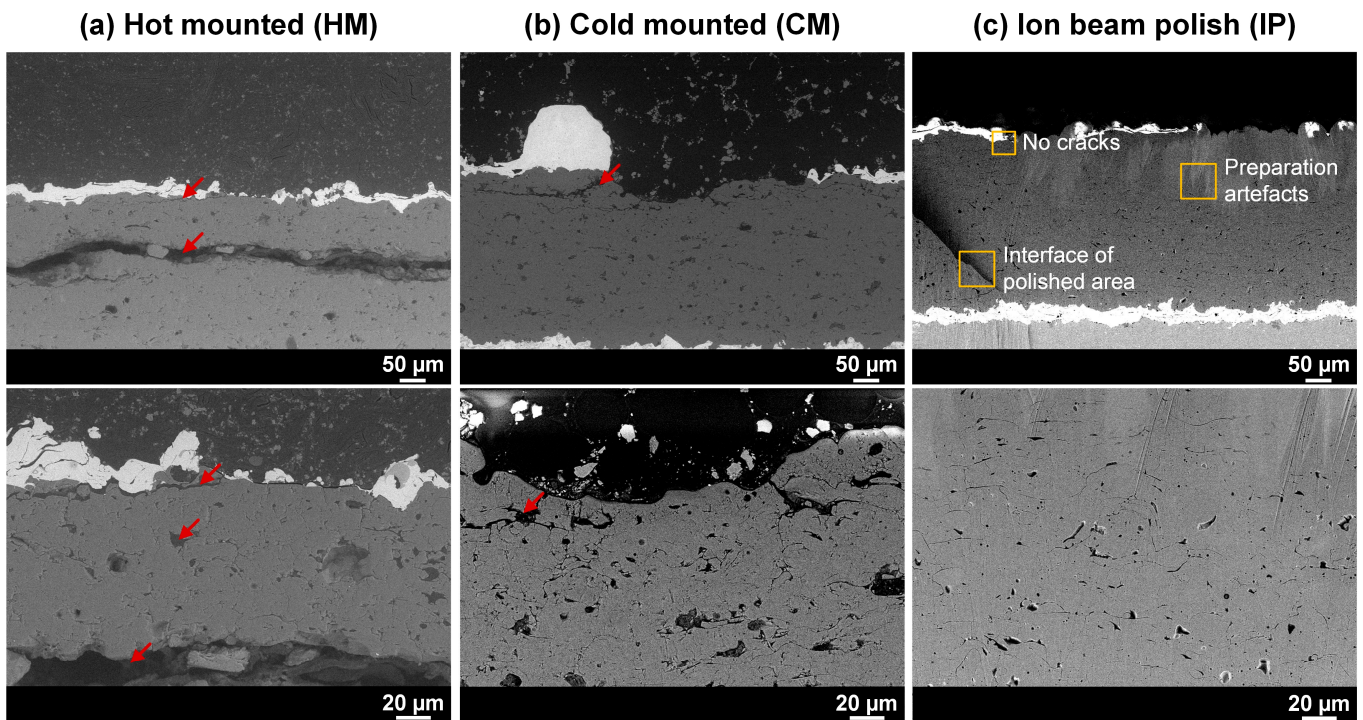


**Figure 12.** Overview of the differently prepared arc-sprayed coatings in the laser texturing area (top) and a more detailed view for plasma-sprayed Al<sub>2</sub>O<sub>3</sub> (bottom). (a) Hot-mounted specimens (HM), (b) cold-mounted specimens (CM) and (c) ion beam polished (IP) specimens. Red arrows mark characteristic, probably critical features such as cracks near the interfaces or the laser trace. Yellow boxes highlight characteristics of IP specimens.

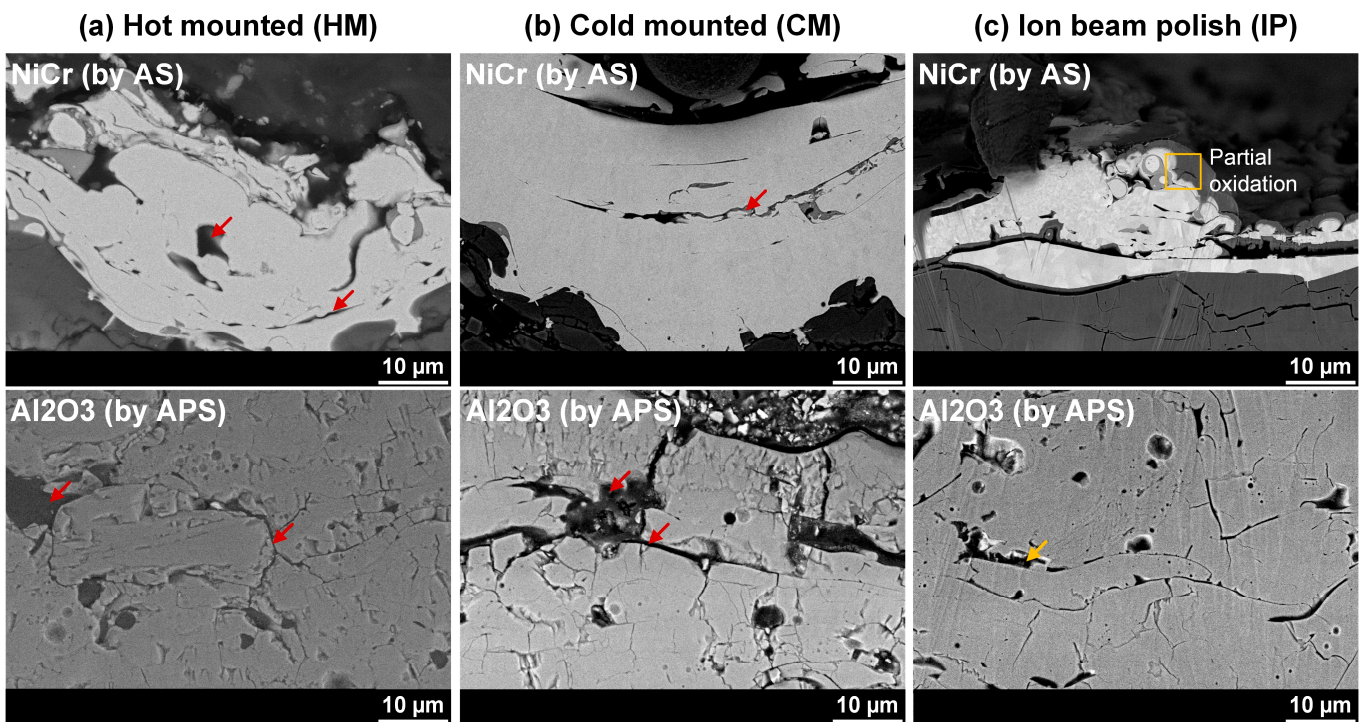


**Figure 13.** Detailed view with higher magnification for arc-sprayed NiCr (top) and the underlying plasma-sprayed Al<sub>2</sub>O<sub>3</sub> (bottom). (a) Hot-mounted specimens (HM), (b) cold-mounted specimens (CM) and (c) ion beam polished (IP) specimens. Red arrows mark characteristic, probably critical features such as cracks. Yellow boxes highlight characteristics of IP specimens.

Furthermore, the characteristics of the coatings differ depending on the material. For example, the basic dendritic structures of the NiCr splats can already be recognized at the CM samples, while they can be seen in their entirety after IP preparation. The interparticle boundaries are characterized by larger grains compared with the interior of the splats. Such subtleties cannot be identified for HM. Another peculiarity for IP is the partial oxidation at the edge of the splats. In contrast, the CM samples are the only ones that do not show major material separations at the particle boundaries. For Al<sub>2</sub>O<sub>3</sub>, a homogeneous coating with a finer structure is basically observed for IP compared with HM and CM, which do not differ to a great extent, just as for Figure 12.

### 3.2.2. Chemical and Quantitative Differences

Figure 14 shows the local chemical composition of the differently prepared samples for NiCr. The samples for HM and CM hardly differ from each other in this respect. They are both characterized by a uniform distribution of the alloying elements. Occasionally, lamellar Cr-based oxides are recognizable for HM and partly also for CM. In contrast, spherical oxides are recognizable for IP, which also contain Al in some cases.

Table 3 shows the content of defects determined for the differently prepared samples.

**Table 3.** Content of defects (porosity, oxides, and cracks) in % for arc-sprayed Variations 1 and 2 depending on sample preparation method.

Specimen Defect Content in %	Hot-Mounted (HM)		Cold-Mounted (CM) *		Ion Beam Polish (IP)	
	Al <sub>2</sub> O <sub>3</sub> (APS)	NiCr (AS)	Al <sub>2</sub> O <sub>3</sub> (APS)	NiCr (AS)	Al <sub>2</sub> O <sub>3</sub> (APS)	NiCr (AS)
Variation 1 (S11)	10.9 ± 2.8	6.7 ± 2.2	8.0 ± 1.1	3.9 ± 0.9	2.1	4.5
Variation 2 (S12)	15.8 ± 5.0	3.0 ± 0.2	4.2 ± 0.3	2.8 ± 0.3	4.9	3.1

\* Defect content for plasma-sprayed reference coatings. NiCr: 36.5 ± 5.8% (oxidation-dominated, cf. Figure 1). Al<sub>2</sub>O<sub>3</sub>: 8.9 ± 3.2% (porosity-dominated). These numbers should be compared with the arc-sprayed and CM-prepared specimens due to the same preparation.

Basically, the trends of the oxygen measurements in section “Oxygen Content” were confirmed. The NiCr coatings for Variation 2 have less defects, irrespective of the preparation method. Additionally, the arc-sprayed Variations show far lower numbers compared with the plasma-sprayed reference coatings. In fact, the difference in coating build-up and hence domination of the defect content by oxidation must be considered for the reference coatings. For Al<sub>2</sub>O<sub>3</sub>, this statement cannot be made in general, but these coatings were not part of this parameter determination study and had already been prepared prior to the arc spray experiments. However, it is clearly evident that the CM and IP preparation methods provide largely comparable results for both materials, taking into account the standard deviations. Compared with CM and IP, analysis results and standard deviations determined differ greatly for HM preparation, especially for Al<sub>2</sub>O<sub>3</sub>.

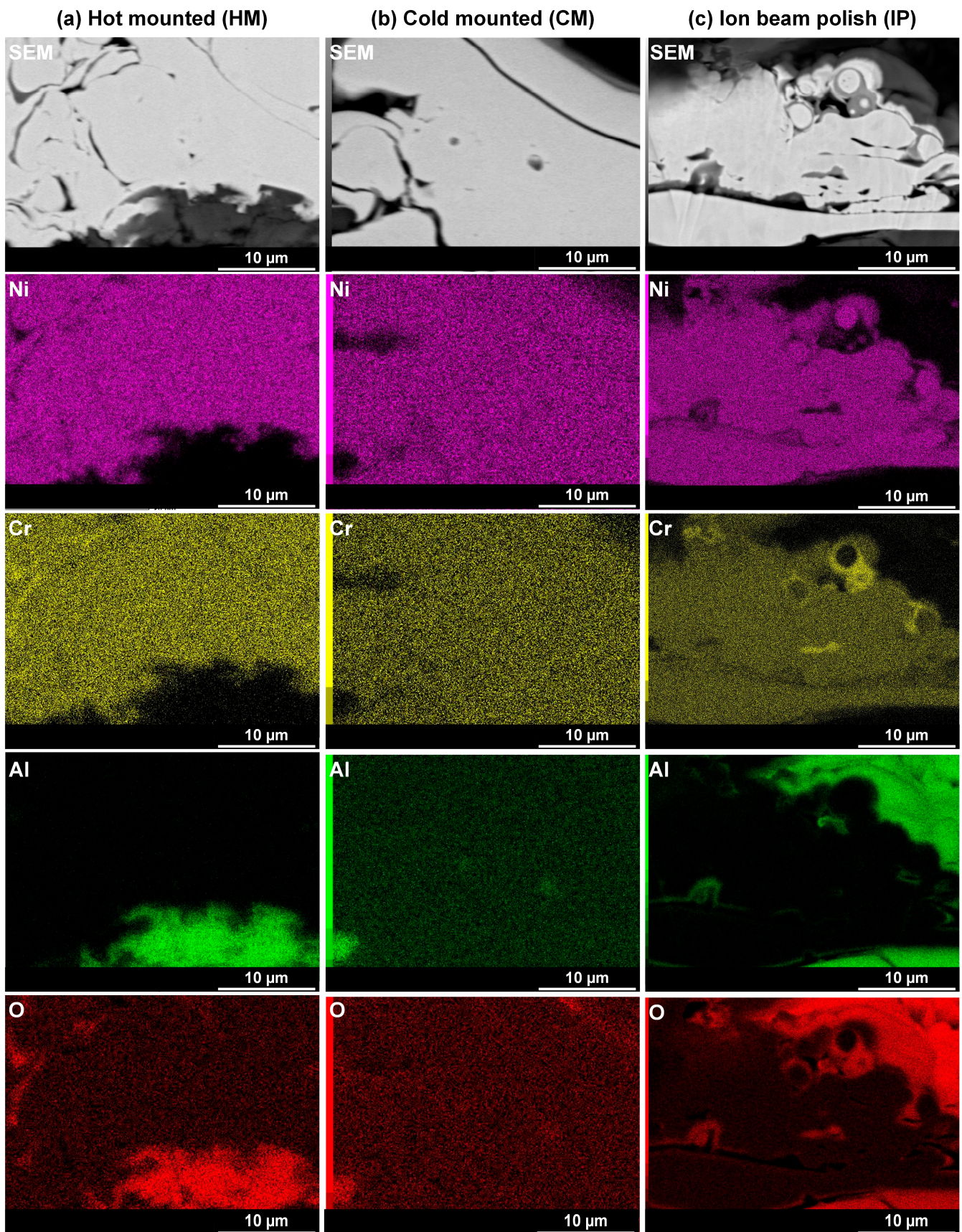


**Figure 14.** EDX-Analyses of the arc-sprayed NiCr coatings regarding the elements Ni, Cr, Al, and O. (a) Hot-mounted specimens (HM), (b) cold-mounted specimens (CM) and (c) ion beam-polished (IP) specimens.

#### 4. Discussion

Similar to the results section, the discussion will also be divided. While in the first section of the discussion the coatings and their functional properties will be evaluated, the heating elements in their entirety will be discussed in the second section. The various preparation methods will be evaluated in the final section of the discussion.

##### 4.1. Evaluation of the Arc-Sprayed Coatings

In case of using NiCr as coating material, it was not clear whether the changes in the spraying process would be sufficient for the coatings to meet the previously defined requirements, such as the specific coating mass or the resistivity of the finally textured heating elements, so that the arc-sprayed coatings could eventually be equivalent to the plasma-sprayed reference coatings.

The parameter sets were investigated directly after the spraying process by immediate analyses of coating mass, thickness, surface quality, and specific resistivity. In particular, the relationship between a high specific conductivity or a low specific resistivity and minor quantities of coating defects such as oxides and pores confirmed this approach, which is displayed in Figure 15. The primary gas mixtures of pure nitrogen as well as nitrogen and 4% of hydrogen can be regarded as the largest factor for the reduction in oxygen content in all the specimens. In terms of oxidation, all coatings are superior to the reference coatings. This fact can be attributed mostly to the shroud effect. The shroud effect describes that particles exhibit less oxidation by the use of inert gases and their mixtures due to protection from the atmosphere [7]. As assumed, the specific resistivity decreases almost linearly in dependence of the measured oxide content, see Figure 15.

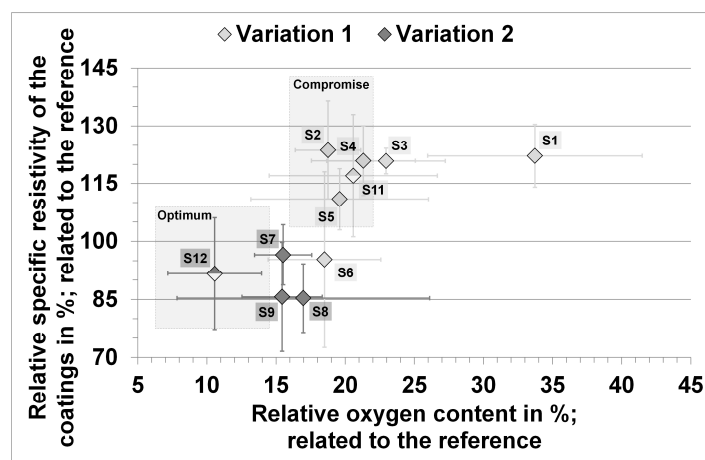


**Figure 15.** Relationship between the relative oxygen content of the arc-sprayed coatings and the relative resistivity of the arc-sprayed coatings; related to the value of the reference coatings (APS; REF  $\cong$  100%).

Furthermore, the change in air cap and thus gas flow largely influences the results of Variation 1 samples, compare S1 and S2 in Figure 15. The use of additional hydrogen (S3–S9) should have further reduced oxidation and promoted an increase in elastic energy of the particles. However, the samples S3 and S2 coincide partly regarding their oxygen content and specific resistivity. The subsequent reduction in stand-off distance from 120 mm (S3) to 60 mm (S6) changes this to a certain extent, i.e., oxygen content and specific resistivity both decrease. Yet, it must be noted, that the shortest stand-off distance does not lead to reproducible results anymore, which is proven by the high standard deviation of the resistivity and the irregular, partially stained surface. Considering these results, the optimum coating quality for Variation 1 is reached by specimens of S5 and S11, which almost equal the reference coatings considering the specific resistivity.

In the case of Variation 2, the gas flow optimization by change in the air cap and the use of nitrogen as secondary shielding gas further enhanced the gas shroud effect. As already described for Variation 1, reproducible results cannot be achieved with the lowest spray distance. Thus, the specimens of S8 and S12 of Variation 2 reach the most suitable coating properties regarding the whole test series, compare Figures 8 and 15, Table 2.

Despite the superior coating properties achieved by arc spraying, a certain amount of cracking was observed in the arc-sprayed coatings as well as in the ceramic coatings underneath. A reason for cracking can be residual stresses, resulting from the superposition of quenching stresses by subsequently evolving cooling stresses [7]. Nevertheless, it is more likely that the preparation of the specimens has the greatest influence on the occurrence of these cracks since the influence of residual stresses is weakened by the use of alternative gas mixtures [7]. Hot mounting takes place under increased temperature and pressure, while the subsequent grinding and polishing processes artificially expand potential cracks or even particle boundaries. This shall be further discussed in Section 4.3. Findings from the advanced analytical methods.

#### 4.2. Suitability of the Coatings as Heating Units

Aside from reaching very positive results regarding the coating quality, the coatings needed to be approved for use as heating units by measuring their electric characteristics.

Due to the very low oxygen contents and the uniform surfaces, see Figures 5, 10 and 11a, the coatings could be textured successfully using the same parameters as for the plasma-sprayed reference coatings. Nevertheless, the coatings became visibly darker and more irregular due to the heat input of the texturing process, which indicates a partial surface oxidation of the coatings. This might explain the partial scattering regarding the quantitative evaluation of oxygen content, especially for Variation 1, which was affected more than Variation 2.

As already presented before, the specimens S8 and S12 reach the most suitable coating properties. Furthermore, these specimens also happen to exhibit the lowest TCR values, which are far lower than the reference value, see Figure 16.

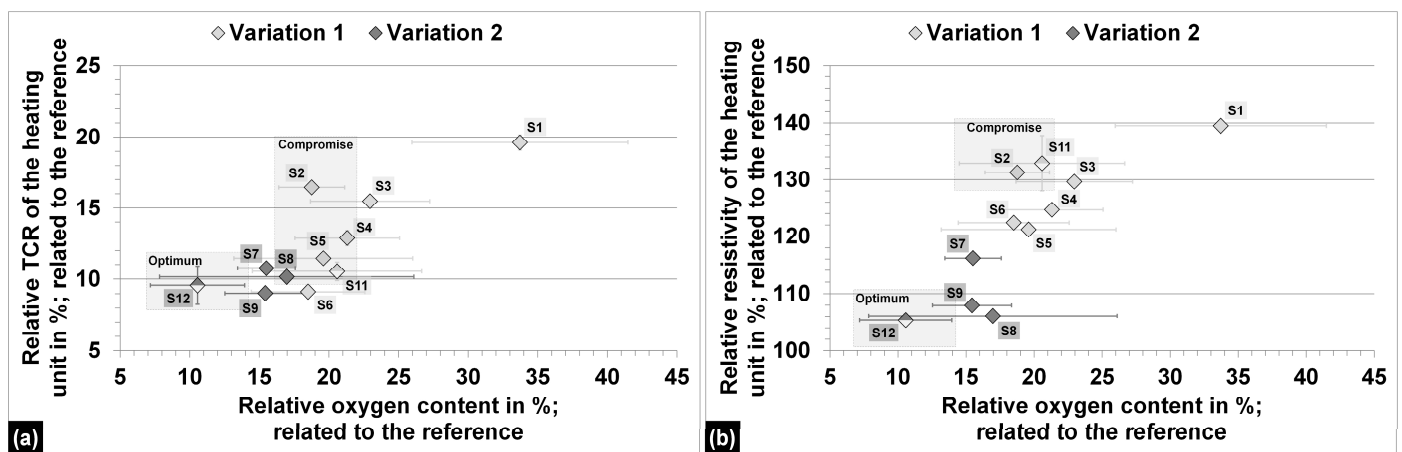


**Figure 16.** Relationship between the relative oxygen content of the arc-sprayed coatings and (a) the relative TCR of the heating units and (b) the relative resistivity of the heating units. All data refer to the reference coating levels (APS; REF  $\hat{=}$  100%). Areas of the best coating properties are highlighted, as well as those which are a compromise between suitable coating properties and good heating characteristics.

Overall, the relationship of coating oxygen content and TCR resembles the findings in the previous chapter. With regard to the use as a heating element, a low TCR is crucial, as it ensures a low temperature dependence of the resistivity [9]. A low TCR therefore also increases the reliability of the heating element to a certain extent. In view of these correlations,

the arc-sprayed coatings can be considered as suitable for this kind of application. This can mainly be attributed to the almost oxide-free structure of these coatings, which in turn, is a result of using wires as feedstock. Coatings manufactured using powder feedstock with particles of varying sizes tend to show a greater scattering in their characteristics due to the different specific surfaces of the particles and thus display a high level of local oxidation.

However, the disadvantage of these very oxide-free coatings is that the resistivity of the heating element is only slightly higher than for the currently used plasma-sprayed reference coatings, see Figure 16b. However, this was to be expected from a physical point of view, since the resistivity of the heating conductor tends to correlate with the specific coating resistivity. For future applications, e.g., for differently designed heating conductor geometries, this could be a problem. Nevertheless, it should be noted that the specified minimum value of resistivity regarding the heating conductor was reached and even slightly exceeded.

In summary, it can be stated that both variations resulted in coatings that can potentially be used for heating elements. While the best coating properties are achieved by secondary atomization in Variation 2, the use of the High Velocity air cap with optimization of the stand-off distance in Variation 1 is a workable compromise, see Figures 15 and 16. Using a High Velocity air cap could provide further advantages, e.g., regarding the coating of modified heating element designs.

#### 4.3. Findings from the Advanced Analytical Methods

First of all, it can be stated that the preparation methods CM and IP have great advantages over HM, especially with respect to the evaluation of ceramic coatings. For example, the previously observed horizontal cracks in the underlying  $\text{Al}_2\text{O}_3$  coating, as already suspected, clearly originate from the preparation method of hot mounting, and could not be observed for the other methods. Only smaller, non-critical material separations near the texturing and at inter-particle boundaries in the NiCr coating were recognizable. The latter probably are a result of the preparation parameters, which have not yet been fully optimized. For example, no variations were made in the preparation voltage for IP. Furthermore, in the case of CM, it must be noted that the materials NiCr and  $\text{Al}_2\text{O}_3$  have very different mechanical properties, e.g., hardness, which strongly affects the preparation. A uniform, optimum mechanical preparation is thus very unlikely. In contrast, IP already shows very good, uniform microstructures for both materials. For  $\text{Al}_2\text{O}_3$  in particular, this manifests in a finer degree of preparation. For NiCr, on the other hand, some small oxidation effects due to IP were detected via EDX and must be taken into account. Furthermore, the origin of the material separations between the splats visible in the IP specimens cannot be clearly explained. On one hand, it is conceivable that already existing weakly bonded areas were artificially widened as a result of the preparation time and voltage. The slight change in the coating oxides chemical composition also suggests this. Accordingly, these facts would require an optimization of the preparation parameters. However, another possibility that must be considered is that arc wire spraying leads to relatively long and large particles compared with, for example, powder-based coating processes. These smaller cracks could therefore also indicate a suboptimal bonding of the rather thin coatings. Reasonably, a superposition of these two effects can therefore be assumed.

Nevertheless, from direct comparison it can be concluded that the preparation by means of IP provides the most reliable and best results, which is also reflected in the quantitative evaluation of the coating defects.

## 5. Conclusions and Outlook

The aims of this study were twofold. On one hand, several mixtures and combinations of alternative pressurizing gases and further process modifications of the arc spray process, such as change in air cap and stand-off distance, were tested to optimize the coating characteristics regarding their use as heating elements. On the other hand, advanced

preparation methods were used in order to quantify the influence of sample preparation on the coating analysis results. The key findings of the study are listed below:

1. The process optimization results demonstrate significantly reduced oxygen contents and improved coating morphologies compared with the currently used plasma-sprayed reference coatings. This also affects the measured defect content overall positively, especially in terms of oxidation. It can be assumed that a further reduction in oxygen content by parameter adjustment alone is difficult to achieve, as a residual amount of oxygen is always present with arc spray processes. However, a change to a modern power source and an improved torch design might improve the coating properties.
2. The improved microstructure positively affects the surface quality and the specific resistivity of the coatings. Nevertheless, some micro cracking was observed inside the arc-sprayed coatings and the ceramic coatings underneath. Although the cracking most probably originates from the preparation of the specimens by hot mounting, as was evident from the comparison of different sample preparation methods, characteristics of the arc spray process must be considered too.
3. Due to the improved surface structure and reduced oxide content, the arc-sprayed specimens can be subsequently textured just as successfully as the plasma-sprayed reference coatings. Moreover, the temperature coefficients of resistance (TCR) and the resistivity of the heating elements were found to be superior to conventionally manufactured coatings.
4. It can be shown that the preparation method is essential regarding the analysis results, especially for ceramic coatings. Compared with hot mounting, cold mounting and ion beam polishing were clearly less influential on the coating characteristics and led to more representative analysis results. The latter allowed a very fine preparation of the coatings, which even provided insights into the dendritic microstructure depending on the position within the coating splats.

The key characteristics of the coatings (adhesive and cohesive), which can be found in the previous figures and tables throughout the manuscript, are summarized again in the following Table 4.

**Table 4.** Adhesive and cohesive key characteristics of the arc-sprayed coatings compared with the plasma-sprayed reference coatings. All relative data refer to reference coating levels (REF  $\hat{=}$  100%).

	Tensile Adhesive Strength in MPa	Defect Content (CM) in %	Relative Oxygen Content in %	Relative Coating Resistivity in %	Relative Heating Unit TCR in %	Relative Heating Unit Resistivity in %
REF ( $\hat{=}$ APS)	22.4 $\pm$ 2.5	36.5 $\pm$ 5.8	100 $\pm$ 14	100 $\pm$ 3	100	100
Variation 1: S11 ( $\hat{=}$ AS)	47.8 $\pm$ 0.6	3.9 $\pm$ 0.9	21 $\pm$ 6	117 $\pm$ 16	11 $\pm$ 1	133 $\pm$ 5
Variation 2: S12 ( $\hat{=}$ AS)		2.8 $\pm$ 0.3	11 $\pm$ 3	92 $\pm$ 14	10 $\pm$ 1	105 $\pm$ 1

The previously listed findings and Table 4 suggest that the improved properties of the arc-sprayed coatings, including superior temperature coefficients of resistance and resistivity, hold promise for potential industrial applications in heating element production. However, the technology requires further validation and additional tests. Future research could include, for example, prototyping and testing the technology on actual heating element components over many load cycles to validate its industrial applicability.

In conclusion, this study successfully optimized the arc spraying process for heating element coatings, demonstrating improved properties and, moreover, highlighted the significance of sample preparation methods in coating analysis.

**Author Contributions:** Conceptualization, K.-M.H. and A.G.; thermal spraying (supervision), W.K.; thermal spraying (supervision and writing), M.H. and B.R.; functional and microstructural coating analyses (supervision, investigation, writing, and visualization), M.H. and B.R.; overall supervision, A.G. All authors have read and agreed to the published version of the manuscript.

**Funding:** This project is/was co-financed by the European Union from the European Regional Development Fund. Operational Program Mecklenburg-Western Pomerania 2014–2020—Investments for Growth and Employment (TBI-V-1-181-VBW-063).

**Institutional Review Board Statement:** Not applicable.

**Informed Consent Statement:** Not applicable.

**Data Availability Statement:** All data that support the findings in this study are available to researchers upon reasonable request.

**Acknowledgments:** The authors would like to thank M. Gey, L.-L. Hütsch, S. Lange, C. Pust, A. Schmidmayer and E. Shirinov (in alphabetical order) for their support with the test materials, the execution of the tests and the evaluation of the results.

**Conflicts of Interest:** The authors declare no conflict of interest. The authors declare that W.K. was not involved in the study design, collection, analysis, interpretation of data, the writing of this article or the decision to submit it for publication.

## References

1. Kim, J.-H.; Lee, M.-H. A Study on Cavitation Erosion and Corrosion Behavior of Al-, Zn-, Cu-, and Fe-Based Coatings Prepared by Arc Spraying. *J. Therm. Spray Technol.* **2010**, *19*, 1224–1230. [CrossRef]
2. GTV Verschleißschutz GmbH; Krebs Korrosionsschutz GmbH Rostock; EEW SPC GmbH. Thermal Sprayed Aluminium: A Brand-New Robot-Based Technological Coating Concept. Available online: <https://www.youtube.com/watch?v=O5v73kPugm0> (accessed on 24 September 2023).
3. Bunel, M.; Borit, F.; Delloro, F.; Jeandin, M.; Bacciochini, A.; Lemeille, P.; Hervé, E.; Meillot, E.; Roche, K.; Surdon, G. Experimental and Numerical Study of the Influence of Powder Characteristics in the Cold Spraying of Al-based Alloys for Additive Manufacturing Using Low-Pressure, Medium-Pressure and High-Pressure Cold Spray Facilities. In *Thermal Spray 2017: Proceedings from the International Thermal Spray Conference, ITSC 2017, Düsseldorf, Germany, 7–9 June 2017*; Agarwal, A., Bolelli, G., Concustell, A., Lau, Y.-C., McDonald, A., Toma, F.-L., Turunen, E., Widener, C.A., Eds.; DVS Media GmbH: Düsseldorf, Germany, 2017; pp. 719–724.
4. Perry, J.; Richer, P.; Jodoin, B.; Matte, E. Pin Fin Array Heat Sinks by Cold Spray Additive Manufacturing: Economics of Powder Recycling. In *Thermal Spray 2018: Proceedings from the International Thermal Spray Conference. ITSC2018, Orlando, Florida, USA, 7–10 May 2018*; Azarmi, F., Balani, K., Li, H., Eden, T., Shinoda, K., Hussain, T., Toma, F.-L., Lau, Y.-C., Veilleux, J., Eds.; ASM International: Almere, The Netherlands, 2018; pp. 179–186.
5. Pawłowski, L. *The Science and Engineering of Thermal Spray Coatings*, 2nd ed.; Wiley: Chichester, UK; Hoboken, NJ, USA, 2008; ISBN 978-0-471-49049-4.
6. Bach, F.-W.; Möhwald, K.; Laarmann, A.; Wenz, T. *Moderne Beschichtungsverfahren: Die Beiträge Dieses Buches Entstammen Einer Fortbildungsveranstaltung der Deutschen Gesellschaft für Materialkunde in Kooperation mit dem Institut für Werkstoffkunde der Universität Hannover und Dessen Geschäftsbereich Fortis in Witten*; Bach, F.-W., Ed.; Wiley-VCH: Weinheim, Germany, 2005; ISBN 3-527-30977-2. (In German)
7. Chráska, P.; Dubsky, J.; Neufuss, K.; Písacka, J. Alumina-base plasma-sprayed materials part I: Phase stability of alumina and alumina-chromia. *J. Therm. Spray Technol.* **1997**, *6*, 320–326. [CrossRef]
8. Müller, J.-H.; Kreye, H. Mikrostruktur und Eigenschaften von thermisch gespritzten Aluminiumoxidschichten. *Schweiss. Schneid.* **2001**, *53*, 336–345.
9. Lindner, H.; Brauer, H.; Lehmann, C. *Handbook of Electrical Engineering and Electronics (Taschenbuch der Elektrotechnik und Elektronik): Mit 99 Tabellen*, 9th ed.; neu bearb. Aufl.; Fachbuchverl. Leipzig im Carl-Hanser-Verl.: München, Germany, 2008; ISBN 9783446414587. (In German)
10. Tejero-Martin, D.; Rezvani Rad, M.; McDonald, A.; Hussain, T. Beyond Traditional Coatings: A Review on Thermal-Sprayed Functional and Smart Coatings. *J. Therm. Spray Technol.* **2019**, *28*, 598–644. [CrossRef]
11. Gärtner, F.; Voyer, J.; Xiumei, Q.; Kreye, H.; Richter, H.J.; Krömmer, W. Neue Herausforderungen für das Draht- und Stabflammspritzen: New Challenges for Wire and Rod Flame Spraying. In *Tagungsunterlagen Kolloquium Hochgeschwindigkeits-Flammspritzen: Proc. HVOF Spraying, 27. and 28. November 2003, Erding*; Heinrich, P., Ed.; Gemeinschaft Thermisches Spritzen e.V.: Unterschleißheim, Germany, 2003; pp. 61–71.
12. Naumenko, D.; Pillai, R.; Chyrkin, A.; Quadackers, W.J. Overview on Recent Developments of Bondcoats for Plasma-Sprayed Thermal Barrier Coatings. *J. Therm. Spray Technol.* **2017**, *26*, 1743–1757. [CrossRef]
13. Fiedler, T.; Rösler, J.; Bäker, M. A new Metallic Thermal Barrier Coating System for Rocket Engines: Failure Mechanisms and Design Guidelines. *J. Therm. Spray Technol.* **2019**, *28*, 1402–1419. [CrossRef]

14. Oksa, M.; Turunen, E.; Suhonen, T.; Varis, T.; Hannula, S.-P. Optimization and Characterization of High Velocity Oxy-fuel Sprayed Coatings: Techniques, Materials, and Applications. *Coatings* **2011**, *1*, 17–52. [[CrossRef](#)]
15. Davis, J.R. *Handbook of Thermal Spray Technology*; Thermal Spray Society; ASM International: Materials Park, OH, USA, 2004; ISBN 0-87170-795-0.
16. Lang, F.; Krömmer, W. Economic and ecological benefits of using gas mixtures for arc spraying. In *Proc. HVOF Spraying, 29. and 30. October 2018, Erding: Colloquium HVOF Spraying/Kolloquium Hochgeschwindigkeits-Flammspritzen*; Penszior, C., Ed.; Gemeinschaft Thermisches Spritzen e.V: Unterschleißheim, Germany, 2015; pp. 79–88.
17. Hauer, M.; Banaschik, R.; Henkel, K.-M. Innovative Quality Assurance of Laser Welded Joints on Arc-sprayed Coatings using Alternative Gas Mixtures: Innovative Qualitätssicherung lasergeschweißter Verbindungen auf lichtbogengespritzten Schichten unter Einsatz alternativer Gasgemische. In *Proc. HVOF Spraying, 25. and 26. October 2018, Erding: Colloquium HVOF Spraying/Kolloquium Hochgeschwindigkeits-Flammspritzen*; Penszior, C., Ed.; Gemeinschaft Thermisches Spritzen e.V: Unterschleißheim, Germany, 2018; pp. 111–122.
18. ASM Technical Books. Accepted Practice for Metallographic Preparation of Thermal Spray Coating Samples. In *Thermal Spray Technology*; ASM Technical Books, Ed.; ASM International: Almere, The Netherlands, 2022; pp. 30–54. ISBN 978-1-62708-428-4.
19. Leistner, E. *Gefügeatlas zur Präparation und Auswertung thermischer Spritzschichten: =Structural Atlas for the Preparation and Evaluation of Thermally Sprayed Coats*; Verl. für Schweißen und Verwandte Verfahren DVS-Verl.: Düsseldorf, Germany, 2001; ISBN 3-87155-197-X.
20. Smith, M.F.; McGuffin, D.T.; Henfling, J.A.; Lenling, W.J. A comparison of techniques for the metallographic preparation of thermal sprayed samples. *J. Therm. Spray Technol.* **1993**, *2*, 287–294. [[CrossRef](#)]
21. JEOL (Germany) GmbH. *The JEOL Cross Section Polisher: The Ultimate SEM Preparation Tool*; Jeol (Germany) GmbH: Freising, Germany, 2016.

**Disclaimer/Publisher’s Note:** The statements, opinions and data contained in all publications are solely those of the individual author(s) and contributor(s) and not of MDPI and/or the editor(s). MDPI and/or the editor(s) disclaim responsibility for any injury to people or property resulting from any ideas, methods, instructions or products referred to in the content.